Influence of the Anion on the Formation of Amorphous Ionically Conducting Lithium Salt Complexes with 18-C-6 and 2.2.2-Cryptand Macrocycles

Rensl E. A. Dillon, Charlotte L. Stern, and Duward F. Shriver*

Department of Chemistry and Materials Research Center, Northwestern University, Evanston, Illinois 60208-3113

Received October 13, 2000. Revised Manuscript Received June 6, 2001

Complexes of lithium salts $LiCF_3SO_3$, LiI, $LiCH_3CO_2$, $LiBF_4$, LiSCN, and $Li[R-NSO_2CF_3]$ with the macrocyclic ligands 18-C-6 and 2.2.2-cryptand were examined by differential scanning calorimetry, infrared and Raman spectroscopy, and complex impedance. The formation of an amorphous phase appears to be facilitated by the presence of an unsymmetrical anion containing an ether oxygen of the type $[R-NSO_2CF_3]^-$. An X-ray crystal structure was determined for $Li[CF_3SO_2N(CH_2)_2OCH_3]$; these data and that for the previously reported $Li[CF_3SO_2N(CH_2)_3OCH_3]$ structure was correlated with the physical properties of their 18-C-6 and 2.2.2-cryptand complexes.

Introduction

The development of high-energy density batteries and electrochromic displays has stimulated the preparation of new solid electrolytes.[1−3] Polymer salt complexes, formed by weakly ion paired salts dissolved in flexible polar polymers are promising electrolyte materials because of their combination of mechanical and electrochemical properties.[4−7] Recently, novel systems including gel electrolytes,[8−10] composite electrolytes,[11−13] rubbery electrolytes,[14−16] molten salts/ionic liquids,[17−19] and hybrid materials[20,21] have been investigated.

In an earlier publication, we described new amorphous electrolytes containing macrocyclic ligands,[22] where cryptand or crown ethers with macrocyclic cavities larger than the diameter of the lithium cation form complexes with $Li[CF_3SO_2N(CH_2)_3OCH_3]$, which exhibit substantial ionic conductivity such as $[Li\subset 18\text{-C-}6][CF_3SO_2N(CH_2)_3OCH_3]$ (where $\subset$ indicates Li^+ inclusion in the crown ether 18-C-6). Initially, we attributed the formation of these amorphous phases to the mismatch between the cavity size of the macrocycle and the diameter of the cation, resulting in multiple conformations of the macrocycle around the lithium cation inhibiting crystallization. This "mismatch concept" is supported by the observation that $Na[CF_3SO_2N(CH_2)_3OCH_3]$ and $K[CF_3SO_2N(CH_2)_3OCH_3]$ salts form amorphous complexes with cryptand or crown ethers that do not match the diameter of the sodium or potassium cations.[23]

Complexes of $Li[CF_3SO_2N(CH_2)_3OCH_3]$ with 18-C-6 and its analogues (analogues of 18-C-6 with the same macrocycle cavity size but different binding affinities and the same binding affinity but different structural features) may form crystalline phases, revealing limitations in the mismatch concept.[24] This observation indicates that the detailed structure of the macrocyclic ligand is an important controlling parameter in the formation of amorphous complexes. Related studies also suggest that the anion plays a significant role in the formation of an amorphous complex. For example, we have found that cryptand and crown ether complexes with the lithium salt, $Li[(CF_3SO_2)_2N]$, are usually

(1) Blonsky, P. M.; Clancy, S.; Hardy, L. C.; Harris, C. S.; Spindler, R.; Tonge, J. S.; Shriver, D. F. *CHEMTECH* **1987**, *17*, 758.
(2) Gray, F. M. *Solid Polymer Electrolytes: Fundamentals and Technological Applications*; VCH Publishers: New York, 1991.
(3) Julien, C.; Nazri, G. *Solid State Batteries: Materials Design and Optimization*; Kluwer Academic Publishers: Boston, 1994.
(4) Fenton, D. E.; Parker, J. M.; Wright, P. V. *Polymer* **1973**, *14*, 589.
(5) Armand, M. B.; Chabagno, J. M.; Duclot, M. J. In *Fast Ion Transport in Solids Electrodes and Electrolytes*; Vashishta, P., Mundy, J. N., Shenoy, G. K., Eds.; Elsevier North-Holland, Inc.: Lake Geneva, 1979.
(6) *Polymer Electrolyte Reviews 1*; MacCallum, J. R., Vincent, C. A., Eds.; Elsevier Science Publishers Ltd.: London, 1987; Vol. 1.
(7) Ratner, M. A.; Shriver, D. F. *Chem. Rev.* **1988**, *88*, 109.
(8) Abraham, K. M.; Alamgir, M. *J. Electrochem. Soc.* **1990**, *137*, 1657.
(9) Choe, H. S.; Carroll, B. G.; Pasquariello, D. M.; Abraham, K. M. *Chem. Mater.* **1997**, *9*, 369.
(10) Ballard, D. G. H.; Cheshire, P.; Mann, T. S.; Przeworski, J. E. *Macromolecules* **1990**, *23*, 1256.
(11) Nagasubramanian, G.; Attia, A. I.; Halpert, G.; Peled, E. *Solid State Ionics* **1993**, *67*, 51.
(12) Appetecchi, G. B.; Croce, F.; Dautzenberg, G.; Mastragostino, M.; Ronci, F.; Scrosati, B.; Soavi, F.; Zanelli, A.; Alessandrini, F.; Prosini, P. P. *J. Electrochem. Soc.* **1998**, *145*, 4126.
(13) Fan, J.; Fedkiw, P. S. *J. Electrochem. Soc.* **1997**, *144*, 399.
(14) Angell, C. A.; Liu, C.; Sanchez, E. *Nature* **1993**, *362*, 137.
(15) Angell, C. A.; Fan, J.; Liu, C.; Lu, Q.; Sanchez, E.; Xu, K. *Solid State Ionics* **1994**, *69*, 343.
(16) Angell, C. A.; Xu, K.; Zhang, S.; Videa, M. *Solid State Ionics* **1996**, *86−88*, 17.
(17) Liu, C.; Angell, C. A. *Solid State Ionics* **1996**, *86−88*, 467.
(18) Watanabe, M.; Yamada, S.; Ogata, N. *Electrochim. Acta* **1995**, *40*, 2285.
(19) Bonhote, P.; Dias, A.; Papageorgiou, N.; Kalyanasundaram, K.; Gratzel, M. *Inorg. Chem.* **1996**, *35*, 1168−1178.
(20) Hu, S.; Fang, S. *Electrochim. Acta* **1999**, *44*, 2721.
(21) Ito, K.; Ohno, H. *Electrochim. Acta* **1998**, *43*, 1247.
(22) Dillon, R. E.; Shriver, D. F. In *Materials Research Society*; Ginley, D. S., Doughty, D. H., Scrosati, B., Takamura, T., Zhang, Z., Eds.; Materials Research Society: Boston, 1998; Vol. 496.
(23) Dillon, R. E. A.; Shriver, D. F. *Solid State Ionics* **2000**, *132*, 93.
(24) Dillon, R. E. A.; Shriver, D. F. *Solid State Ionics* **2000**, *133*, 239.

10.1021/cm000824f CCC: $20.00
Published on Web 07/12/2001

crystalline, in contrast to the amorphous character of $Li[CF_3SO_2N(CH_2)_3OCH_3]$ complexes.[25] This result led to the examination of vibrational and X-ray single-crystal structural data of $Li[CF_3SO_2N(CH_2)_3OCH_3]$[26] and $Li[(CF_3SO_2)_2N]$[27] to provide insight into the lithium cation interaction with the respective anions. These results are compared to the related study in which we examined the lithium cation position within the macrocyclic ligand and the residual interaction between the anion and the cation for $[Li\subset 12\text{-}C\text{-}4][CF_3SO_2N(CH_2)_3OCH_3]$,[26] $[Li\subset 2.2.2][(CF_3SO_2)_2N]$,[28] and $[Li\subset(12\text{-}C\text{-}4)_2][(CF_3SO_2)_2N]$[28] complexes. We tentatively attributed the formation of crystalline $Li[(CF_3SO_2)_2N]$ complexes with the symmetry and weak basicity of the $[(CF_3SO_2)_2N]^-$ anion. The crystal structures indicate (i) the weak interaction between the lithium cation and the anion in the salt structure, (ii) the lithium cation residence in the macrocycle ligand and the complete disassociation of the anion, and (iii) the structural features of the anion that lend itself to crystallization of its complexes.

As a result of all our work to date, we suggest that the formation of these amorphous phases may be attributed to the binding affinity between the macrocycle and the cation and the structure of the macrocycle ligand and anion. These features result in multiple conformations of the complex, resulting from lithium cation interaction within the macrocycle and the anion, which promote long-range disorder in the material. These ideas have been supported by solid-state NMR data that show that in the $[Li\subset 2.2.2][CF_3SO_2N(CH_2)_3OCH_3]$ complex, transport of lithium cations takes place through averaged residence time fractions of 77% to 23% on the anion and macrocycle, respectively.[29]

To date, our hypothesis on the formation of amorphous lithium salt complexes with macrocyclic ligands has been tested on two lithium salts, $Li[CF_3SO_2N(CH_2)_2OCH_3]$ and $Li[(CF_3SO_2)_2N]$, with mixed results. The present investigation explores the role of the anion in more detail to determine the role of the anion in the formation of amorphous complexes with substantial ionic conductivity. Specifically, 18-C-6 and 2.2.2-cryptand complexes of $LiCF_3SO_3$, LiI, $LiCH_3CO_2$, $LiBF_4$, LiSCN, and $Li[R-NSO_2CF_3]$ (Figure 1) were prepared and characterized by thermal analysis, spectroscopy, and ionic conductivity. In addition, we examine the X-ray single-crystal structural data of $Li[CF_3SO_2N(CH_2)_2OCH_3]$ and compare it to the $Li[CF_3SO_2N(CH_2)_3OCH_3]$ structure to elucidate the differences between each salts' 18-C-6 and 2.2.2-cryptand complexes.

Experimental Section

Syntheses were carried out under an inert atmosphere of dry nitrogen in a Schlenk line. The salts $LiCF_3SO_3$, $LiCH_3CO_2$, $LiBF_4$, and LiSCN were purchased from Aldrich and dried under high vacuum at elevated temperatures for 3 days. LiI (ampule under Argon, water < 100 ppm, purity 99.999%) was purchased from Aldrich and used as received. $Li[(CF_3SO_2)_2N]$ (3 M) was dried at 150 °C for 2 days at 8×10^{-6} Torr. The dry salts were handled in a drybox. Infrared spectra confirmed the absence of water. $Li[CF_3SO_2N(CH_2)_3OCH_3]$ was prepared as previously described[30] and salts of the general formula $Li[R-NSO_2CF_3]$ {$Li[CF_3SO_2N(CH_2)_2OCH_3]$, $Li[CF_3SO_2NCH_2CH(OCH_3)_2]$, $Li[CF_3SO_2NCH_2CH_3]$, $Li[CF_3SO_2NCH_2CF_3]$, $Li[CF_3SO_2NCH(CH_3)_2]$, $Li[CF_3SO_2NCH(CH_3)CH_2OCH_3]$, $Li[CF_3SO_2NCH_2(C_4H_7O)]$, and $Li[CF_3SO_2NCH_2$-18-C-6]} were prepared by analogous routes using $(CF_3SO_2)_2O$ or CF_3SO_2Cl and the specific amine $R-NH_2$.[31]

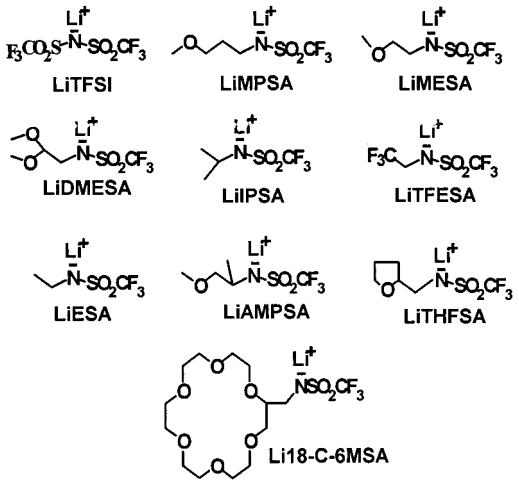

Figure 1. Lithium salts with the formula $Li[R-NSO_2CF_3]$.

Macrocycles. 18-C-6 and 2.2.2-cryptand were purchased from Aldrich; 18-C-6 (1,4,7,10,13,16-hexaoxacyclooctadecane) was sublimed at 35 °C (1×10^{-1} Torr), and 2.2.2-cryptand (4,7,13,16,21,24-hexaoxa-1,10-diazabicyclo[8.8.8]hexocosane was dried on a high vacuum line at 30 °C (8×10^{-6} Torr).

Complex Formation. Under an inert atmosphere of dry nitrogen, equimolar quantities of the lithium salt and the macrocycle were heated until molten and then quenched at 0 °C. The samples were judged free of residual solvent and water by infrared spectroscopy and they were stored in a dry inert atmosphere.

Characterization. Mass spectra were obtained at the Midwest Center for Mass Spectrometry (University of Nebraska, Lincoln) or the Analytical Service Laboratory at Northwestern University. NMR spectra were recorded on a Varian Gemini 300 MHz NMR spectrometer. ^1H NMR spectra were referenced to $CDCl_3$, CD_2Cl_2, or CD_3CN; ^{19}F NMR spectra were referenced to CCl_3F. Elemental analyses were performed by Oneida Research Services, Inc. (Whitesboro, New York) or Midwest Microlab (Indianapolis, IN).

Differential scanning calorimetry (DSC) was performed on a Perkin-Elmer Pyris 1 instrument on samples loaded in an inert atmosphere into hermetically sealed aluminum pans. A stable baseline was observed over the temperature range −100 °C to 200 °C and the instrument was calibrated with indium and decane. All transitions were recorded at a heating rate of 40 °C/min. Glass transitions are assigned at the middle of the transition. Melting and cold crystallization temperatures are assigned to the onset of the transitions. Amorphous materials exhibited a glass transition as the only thermal transition in the first DSC scan. Crystalline samples were melted and then quenched to −100 °C at 200 °C/min in an attempt to form amorphous materials.

Raman spectra were recorded on a FT-Raman spectrometer with excitation by a Nd:YAG laser at 1.064 μm on samples in sealed capillary tubes. Amorphous samples exhibited weak broad Raman bands in comparison to the sharper spectra of crystalline samples. The spectral resolution of the interfer-

(25) Dillon, R. E. A.; Shriver, D. F. *Chem. Mater.* **1999**, *11*, 3296.
(26) Dillon, R. E. A.; Stern, C.; Shriver, D. F. *Chem. Mater.* **2000**, *12*, 1122.
(27) Nowinski, J. L.; Lightfoot, P.; Bruce, P. G. *J. Mater. Chem.* **1994**, *4*(10), 1579.
(28) Dillon, R. E. A.; Stern, C.; Shriver, D. F. *Solid State Ionics* **2000**, *133*, 247.
(29) Sigmund, E. E.; Halperin, W. P.; Dillon, R. E. A.; Shriver, D. F., submitted to *Phys. Rev. B*.
(30) Lascaud, S.; Perrier, M.; Vallee, A.; Besner, S.; Prud'homme, J.; Armand, M. *Macromolecules* **1994**, *27*, 7469.
(31) Dillon, R. E. A.; Stern, C.; Shriver, D. F. See the Supporting Information for this manuscript.

Table 1. Crystallographic Data for $Li[CF_3SO_2N(CH_2)_2OCH_3]$

empirical formula	$C_4H_7NSF_3O_3Li$
formula weight	213.10
crystal color, habit	colorless, needle
crystal dimensions	0.20 × 0.05 × 0.01 mm
crystal system	monoclinic
lattice type	C-centered
lattice parameter, *a*	18.969(8) Å
lattice parameter, *b*	8.939(4) Å
lattice parameter, *c*	10.347(4) Å
lattice parameter, β	92.591(7) Å
lattice parameter, *V*	1752.7(11) Å^3
space group	*C*2/*c* (No. 15)
Z value	8
D_{calc}	1.615 g cm^{-3}
*F*000	864.00
μ(Mo Kα)	3.90 cm^{-1}
temperature	−120 °C
R1[a]	0.036
wR2[b]	0.058
goodness of fit indicator	0.87

[a] $R1 = \sum||F_o| - |F_c||/\sum|F_o|$. [b] $wR2 = [(w(F_o^2 - F_c^2)^2)/\sum w(F_o^2)^2]^{1/2}$.

ometer was 4 cm^{-1}. Infrared spectra were recorded on a Bomem MB-100 FTIR spectrometer with 2-cm^{-1} resolution on solutions in 0.1-mm path length CaF_2 solution cells. Alternatively, neat samples of amorphous materials were placed between KBr plates. Crystalline samples were prepared as KBr pellets.

Complex impedance measurements were performed with a Hewlett-Packard 4192A in the frequency range 5 Hz to 13 MHz on samples sandwiched between stainless steel electrodes and annealed for 12−24 h at 100 °C. Data were collected between 100 and 20 °C using a temperature ramp of 0.2 °C/min.

X-ray Crystal Structure of $Li[CF_3SO_2N(CH_2)_2OCH_3]$. A colorless flat-needle crystal of $Li[CF_3SO_2N(CH_2)_2OCH_3]$ was grown by slow diffusion of methylene chloride into a solution of the salt in acetonitrile. A crystal with dimensions of 0.20 × 0.05 × 0.01 mm was mounted using oil (Paratone-N, Exxon) on a glass fiber and transferred to a Bruker SMART-1000 diffractometer with a CCD plate area detector and graphite monochromated Mo Kα radiation. Cell constants and an orientation matrix for data collection corresponded to a C-centered monoclinic cell. A summary of the crystallographic data is given in Table 1. The dimensions of the cell yield a calculated density of 1.62 g cm^{-3} ($Z = 8$ and FW = 213.10). The space group was determined to be *C*2/*c* (#15) on the basis of the systematic absences *hkl*, $h + k \pm 2n$, and *h*0*l*, $l \pm 2n$, packing considerations, statistical analysis of intensity distribution, and the successful solution and refinement of the structure. Data for the structure determination were collected at −120 ± 1 °C to a maximum 2θ value of 56.8° in 0.30° oscillations with 0.3-s exposures. The detector swing angle was 28.00°.

Of the 16 260 reflections collected, 4511 were unique (R_{int} = 0.142). Data were collected and processed using the SMART-NT and SAINT-NT programs (Bruker). The linear absorption coefficient, μ, for Mo Kα radiation is 3.9 cm^{-1}. The data were corrected for Lorentz and polarization effects. An integrated absorption correction was applied (SHELXTL). Maximum and minimum transmission factors were 0.990 and 0.895, respectively.

The structure was solved by direct methods[32] and expanded using Fourier techniques.[33] The non-hydrogen atoms were refined anisotropically. Hydrogen atoms were included in idealized positions but not refined. The final cycle of full-matrix least-squares refinement on F^2 was based on 716 observed reflections ($I > 2.5\sigma(I)$) and 118 variable parameters and converged (largest parameter shift was 0.00 times its esd) with unweighted and weighted agreement factors of R1 = 0.036 and wR2 = 0.058. The standard deviation of an observation of unit weight was 0.87 (goodness fit factor). The weighting scheme was based on counting statistics, reflection order in data collection, sin θ/λ, and various classes of indices which showed no unusual trends. The maximum and minimum peaks on the final difference Fourier map corresponded to 0.33 and −0.33 e$^-$/A^3, respectively. Neutral atom scattering factors were taken from Cromer and Waber.[34] Anomalous dispersion effects were included in F_{calc}.[35] All calculations were performed using the Texsan crystallographic software package of Molecular Structure Corporation.[36]

Table 2. Thermal Data of $[Li^+\subset$18-C-6$][A^-]$ Complexes[a]

lithium salts	T_g	T_c	T_m	T_g*	T_c	T_m*
$LiCF_3SO_3$	−38		57	−34	28	51
LiI			128	−14	14	125
[b]$LiCH_3CO_2$						
$LiBF_4$			76	−40	16	74
LiSCN			103		10	40, 102
LiMPSA	−31					
[c]LiMESA			41	−55		
LiDMESA	−37					
LiAMPSA	−58	2	35	−48		
LiTHFSA	−31					
Li18−C-6MSA	−17					
LiTFSI	−53		36	−50	−19	36
LiIPSA	−67	−32	37, 107	−35	52	95
LiESA	−53		74	−38		
LiTFESA	−44					

[a] T_g(°C), glass transition temperature. T_g*(°C), glass transition temperature after quenching. T_m(°C), melting temperature. T_m*(°C), melting temperature after quenching. T_c(°C), cold crystallization temperature. T_c*(°C), cold crystallization temperature after quenching. [b] Complex not formed. [c] Initially complex not formed.

Results and Discussion

Thermal Analysis. The lithium salts LiOTf, LiI, $LiBF_4$, and LiSCN form crystalline complexes with 18-C-6 (Table 2). 18-C-6 complexes of LiOTf, LiI, and $LiBF_4$ were quenched from the molten state to form transient amorphous phases. The DSC data indicate that LiOAc and 18-C-6 do not form a complex because the melting point of the "mixture" is identical to that of 18-C-6. More promising results were obtained for combinations of 18-C-6 with $Li[R-NSO_2CF_3]$ salts. Including quenched samples, 8 of the 10 lithium salts form amorphous complexes with 18-C-6. For the purpose of this discussion we have divided the $Li[R-NSO_2CF_3]$ salts into two groups, anions with ether oxygen substituents: ($Li[CF_3SO_2N(CH_2)_3OCH_3]$, $Li[CF_3SO_2N(CH_2)_2OCH_3]$, $Li[CF_3SO_2NCH_2CH(OCH_3)_2]$, $Li[CF_3SO_2NCH(CH_3)CH_2OCH_3]$, $Li[CF_3SO_2NCH_2(C_4H_7O)]$, and $Li[CF_3SO_2NCH_2$-18-C-6]) and those without an ether oxygen substituent ($Li[(CF_3SO_2)_2N]$, $Li[CF_3SO_2NCH_2CH_3]$, $Li[CF_3SO_2NCH_2CF_3]$, and $Li[CF_3SO_2NCH(CH_3)_2]$). Four of the six anions with ether oxygen substituents are amorphous when synthesized and after quenching the salts $Li[CF_3SO_2N(CH_2)_2OCH_3]$ and $Li[CF_3SO_2NCH(CH_3)CH_2OCH_3]$ form amorphous phases with 18-C-6. Interestingly, $Li[CF_3SO_2$-

(32) Altomare, A.; Cascarano, M.; Giacovazzo, C.; Guagliardi, A. *J. Appl. Crystallogr.* **1993**, *26*, 343.
(33) Beurskens, P. T.; Admiral, G.; Beurskens, G.; Bosman, W. P.; Gelder, R. D.; Israel, R.; Smits, J. M. M. *The DIRDIF-94 Program System;* Technical Report of the Crystallography Laboratory; University of Nijmegen, 1994.
(34) Cromer, D. T.; Waber, J. T. *International Tables for X-ray Crystallography*; The Kynoch Press: Birmingham, 1974; Vol. IV.
(35) Ibers, J. A.; Hamilton, W. C. *Acta Crystallogr.* **1964**, *17*, 781.
(36) *Texsan, for Windows 1.05: Crystal Structure Analysis Package;* Molecular Structure Corporation: The Woodlands, TX, 1997.

Table 3. Thermal Data of [Li$^+$⊂2.2.2][A$^-$] Complexes

lithium salts	T_g	T_m	T_g*	T_c	T_m*
$LiCF_3SO_3$		55, 184, 199			26, 51, 183, 198
[b]LiI					
[b]$LiCH_3CO_2$					
$LiBF_4$		65, 72			64
LiSCN		78, 95		71	51, 97
LiMPSA	−50				
LiMESA		57	−47		
LiDMESA		28	−49		
LiAMPSA	−41				
LiTHFSA		54	−38		
Li18-C-6MSA	−30				
LiTFSI		61, 129			61, 126
LiIPSA		68	−41	10	66
LiESA		66	−46	4	65
LiTFESA		73	−48	8	71

[a] T_g(°C), glass transition temperature. T_g*(°C), glass transition temperature after quenching. T_m(°C), melting temperature. T_m*(°C), melting temperature after quenching. T_c(°C), cold crystallization temperature. T_c*(°C), cold crystallization temperature after quenching. [b] Complex not formed.

$N(CH_2)_2OCH_3$] does not form a complex with 18-C-6. This is surprising because this salt differs by only one methylene group relative to Li[$CF_3SO_2N(CH_2)_3OCH_3$]. In the group of anions without ether oxygen substituents both Li[$(CF_3SO_2)_2N$] and Li[$CF_3SO_2NCH(CH_3)_2$] form a mixture of crystalline and amorphous phase complexes with 18-C-6 before and after quenching.

Thermal data in Table 3 indicate that the lithium salts LiOTf, $LiBF_4$, and LiSCN form crystalline complexes (multiple melting points suggests the formation of multiple discrete complexes) with 2.2.2-cryptand. Unlike 18-C-6 complexes, there were no indications of transient amorphous phases upon quenching. Both LiI and LiOAc do not form complexes with 2.2.2-cryptand despite the expected higher binding affinity of 2.2.2-cryptand in comparison to that of 18-C-6. Three 2.2.2-cryptand complexes with salts having the general formula Li[R−NSO_2CF_3] produced amorphous phases, and three others formed amorphous phases upon quenching the melt. These six complexes contain lithium salts with an ether oxygen substituent in the anion and suggest that these anions inhibit crystallization. Conversely, the non-ether-oxygen-containing anions produce crystalline complexes; however, after quenching from the melt dual phase samples are observed.

The thermal data in Tables 2 and 3 strongly suggest that amorphous complexes are formed either spontaneously or after quenching of Li[R−NSO_2CF_3] salts in contrast to $LiCF_3SO_3$, LiI, $LiCH_3CO_2$, $LiBF_4$, and LiSCN salts. Empirical observations suggest that crystallization is inhibited in these complexes because nuclei fail to form in the extremely viscous molten complex upon cooling.[37] Furthermore, Li[R−NSO_2CF_3] salts which contain an ether oxygen within the anion may form amorphous complexes due to the flexibility of the ether oxygen in the anion which may induce disorder.

Raman Spectroscopy of Anion Modes. The strongest band in the Raman spectra of the Li[R−NSO_2CF_3] salts and that of $LiCF_3SO_3$ is assigned to a symmetric deformation mode, δ_s CF_3, in the range 747−777 cm^{-1} (Table 4).[38,39] Among these, the lowest frequency, 747 cm^{-1}, occurs for the salt, Li[$(CF_3SO_2)_2N$] and Li[$CF_3SO_2NCH_2$-18-C-6]. The [$(CF_3SO_2)_2N$]$^-$ anion is arguably the most weakly basic[40] of the anions in Table 4. Rey and co-workers observed that Li[$(CF_3SO_2)_2N$] poly(ethylene oxide) (PEO) complexes exhibit a δ_s CF_3 Raman band at lower frequency (≈741 cm^{-1}) than that of the pure Li[$(CF_3SO_2)_2N$] salt (747 cm^{-1}).[41,42] Similar results were obtained in the present investigation, as shown in Table 4. Upon complex formation with 18-C-6, the δ_s CF_3 bands are usually shifted to lower frequency with the exception of the Li[$CF_3SO_2N(CH_2)_2$-OCH_3] result which does not form a complex as indicated by DSC data in Table 3. The δ_s CF_3 Raman bands, for the lithium salts complexed with 2.2.2-cryptand, shift to a lower wavenumber relative to the δ_s CF_3 bands of 18-C-6 complexes. This difference is attributed to the more effective encapsulation of the lithium cation by the 2.2.2-cryptand, resulting in negligible Li^+ to [R−NSO_2-CF_3]$^-$ interaction. With one exception the formation of 2.2.2-cryptand complexes results in significant changes in the δ_s CF_3 bands of 13−18 cm^{-1}. The one exception, [Li⊂2.2.2][$N(SO_2CF_3)_2$], exhibits a small 7-cm^{-1} perturbation from the pure salt. This result supports the assertion that the [$N(SO_2CF_3)_2$]$^-$ anion is weakly basic so complexation of the cation does not significantly change the anion environment.

A new Raman band at ≈860 cm^{-1} (Table 4) is observed in the spectra of the complexes; this was originally attributed to a symmetric ring breathing motion of crown ether oxygens surrounding solvated cations.[43] However, similar bands were reported by Papke[44,45] for simple polymer salt complexes and these were assigned to a combination of ring breathing motion and CH_2 rocking modes of the host polymer. Subsequently, Frech and Huang[46] determined the spectra of salt complexes with deuterated diglyme and they suggest that the intense band at ≈860 cm^{-1} is primarily a CH_2 rocking vibration. Whatever the detailed origin, it is clear that the 860-cm^{-1} band is associated with complex formation.[47] The results in Table 4 produce three inconsistent values that require further discussion. The first suggests that a complex is formed between Li[$CF_3SO_2N(CH_2)_2OCH_3$] and 18-C-6; however, this is inconsistent with the thermal and δ_s CF_3 Raman evidence. Apparently, the band at 868 cm^{-1} is a feature in the spectrum of the pure salt. A detailed assignment of the 848-cm^{-1} band for [Li⊂18-C-6][$CF_3SO_2NCH_2CH_3$] has not been established but infrared data suggest that this band is associated with complexation, albeit at a lower wavenumber than expected. The third inconsistency, the 820-cm^{-1} band associated with [Li⊂18-C-6]-

(37) Angell, C. A.. *J. Res. Natl. Inst. Stand. Technol.* **1997**, *102*, 171.
(38) Ferry, A.; Doeff, M. M.; De Jonghe, L. C. *J. Electrochem. Soc.* **1998**, *145*, 1586.
(39) Wen, S. J.; Richardson, T. J.; Ghantous, D. I.; Striebel, K. A.; Ross, P. N.; Cairns, E. J. *J. Electroanal. Chem.* **1996**, *408*, 113−118.
(40) Vallee, A.; Besner, S.; Prud'homme, J. *Electrochim. Acta.* **1992**, *37*, 1579.
(41) Rey, I.; Lassegues, J. C.; Grondin, J.; Servant, L. *Electrochim. Acta.* **1998**, *43*, 1505.
(42) Rey, I.; Johansson, P.; Lindgren, J.; Lassegues, J. C.; Grondin, J.; Servant, L. *J. Phys. Chem.* **1998**, *102*, 3249.
(43) Sato, H.; Kusumoto, Y. *Chem. Lett.* **1978**, 635.
(44) Papke, B. L.; Ratner, M. A.; Shriver, D. F. *J. Phys. Chem. Solids* **1981**, *42*, 493.
(45) Papke, B. L.; Ratner, M. A.; Shriver, D. F. *J. Electrochem. Soc.* **1982**, *129*, 1434.
(46) Frech, R.; Huang, W. *Macromolecules* **1995**, *28*, 1246.
(47) Kasatani, K.; Sato, H. *Chem. Lett.* **1986**, 991−994.

Table 4. Raman Frequencies and Vibrational Assignments for the δ_s CF_3 Modes in Li[R−NSO_2CF_3], $LiCF_3SO_3$, [Li⊂18-C-6], and [Li⊂2.2.2] Complexes, the ν_{srb} CH_2−O[a]

lithium salts	Li[R−NSO_2CF_3] and $LiCF_3SO_3$ δ_s CF_3 (vs) (cm^{-1})	[Li⊂18-C-6] δ_s CF_3 (vs) (cm^{-1})	[Li⊂2.2.2] δ_s CF_3 (vs) (cm^{-1})	[Li⊂18-C-6] ν_{srb} CH_2−O (s) (cm^{-1})	[Li⊂2.2.2] ν_{srb} CH_2−O (s) (cm^{-1})
LiTFSI	747	742	740	860	852
LiMPSA	751	746	738	864	846
LiMESA	753	753	739	[b]**868**	850
LiDMESA	755	748	739	858	842
LiIPSA	753	746	738	860	843
LiTFESA	762	748	744	862	842
LiESA	756	746	738	848	842
LiAMPSA	755	750	739	[b]**820**	[c]**842, 826**
LiTHFSA	754	747	738	861	841
Li18-C-6MSA	747	NA	NA	NA	NA
$LiCF_3SO_3$	777	[c]**763, 753**	[c]**752, 735**	857	841

[a] Assignments: δ (bending), ν (stretching). The subscripts "s" and "srb" denote symmetric and symmetric ring breathing motions, respectively. Band intensities: s (strong), vs (very strong). NA: Not available. [b] The bands at 868 cm^{-1} and at 820 cm^{-1} are found in the pure salt. [c] The origin of peak splitting is unknown.

$[CF_3SO_2NCH(CH_3)CH_2OCH_3]$, is revealed by a comparison to the spectra of the pure salt but the small band at 860 cm^{-1} is not definitive for this complex.

In contrast with the trends for crown systems, a new low-frequency band at ≈840 cm^{-1} (Table 4) is associated with cryptand complex formation. These bands are very consistent throughout the range of anions used (unlike their 18-C-6 analogues). Our group has previously reported similar results for [Na⊂2.2.2] complexes.[48,25]

Ionic Conductivity. The temperature-dependent ionic conductivity of the amorphous 18-C-6 and 2.2.2-cryptand lithium salt complexes can be fit to the semiempirical Vogel−Tamman−Fulcher (VTF) function, which is characteristic of systems where ion motion is coupled to motions of a viscous medium.[49−51]

$$\sigma = AT^{-0.5} \exp[-B/(T - T_0)] \qquad (1)$$

T_0 is a parameter related to the glass transition temperature of the lithium salt complexes and B is related to the fluctuations in the electrolyte matrix that facilitate ion migration. The pre-exponential factor A is dependent on the concentration of charge carriers in the matrix.

In Figure 2, the complexes of the $LiCF_3SO_3$, LiI, $LiCH_3CO_2$, $LiBF_4$, and LiSCN salts are not shown because of their poor conductivity and therefore limited utility. As shown in Figure 2, the highest ionic conductivities are observed for the [Li⊂18-C-6][$(CF_3SO_2)_2N$] and [Li⊂18-C-6][$CF_3SO_2NCH_2CF_3$] complexes. The high ionic conductivities of these salts is attributed to a combination of weakly coordinating anions and low glass transition temperature complexes. Interestingly, both salts do not contain an ether oxygen substituent in their anion. The least conductive complex in Figure 2 is produced by [Li⊂18-C-6][$CF_3SO_2NCH_2$-18-C-6], which clearly has the highest glass transition temperature. However, closer inspection reveals the lithium salt Li[$CF_3SO_2NCH_2$-18-C-6] has nominal ionic conductivity (≈1 × 10^{-8} S cm^{-1} at ≈30 °C and a glass transition temperature of 7 °C).[52] The poor ionic conductivity is attributed to severe restriction of the flexibility afforded by the 18-C-6 substituent attached to the anion. This limitation cannot be completely overcome by the addition of 18-C-6 which lowers the glass transition temperature ≈24 °C. The next lowest ionic conductivity is exhibited by [Li⊂18-C-6][$CF_3SO_2NCH(CH_3)_2$] which forms two phases and which contains a more basic anion. Another interesting observation is the similarity of the conductivities for 18-C-6 complexes which contain an ether oxygen in the anion. Five of the lithium salts in the overlapping conductivity region are salts with an anion that contains an ether substituent.

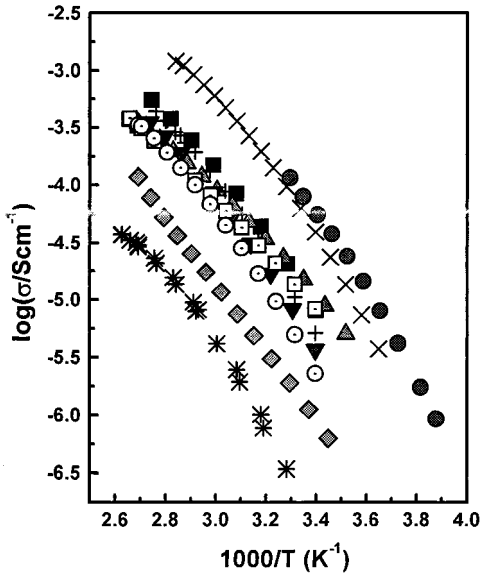

Figure 2. Temperature-dependent ionic conductivities (σ) of 1:1 ratios of Li[R−NSO_2CF_3] complexes with 18-C-6: [LiMPSA⊂18-C-6] (■), [LiTFSI⊂18-C-6] (●), [LiMESA⊂18-C-6] (▲), [LiDMESA⊂18-C-6](▼), [LiIPSA⊂18-C-6] (◆), [LiESA⊂18-C-6] (+), [LiTFESA⊂18-C-6] (×), [Li18−C-6MSA⊂18-C-6] (*), [LiAMPSA⊂18-C-6] (□), and [LiTHFSA⊂18-C-6] (⊙).

The ionic conductivity of the 2.2.2-cryptand complexes (Table 3) are poorer than those of analogous 18-C-6 complexes. This result may reflect strong Li^+ coordination to 2.2.2-cryptand, resulting in higher glass transition temperatures and more crystalline phases. The poorest ionic conductivity in Figure 3 is exhibited by [Li⊂2.2.2][$(CF_3SO_2)_2N$], which is a crystalline material with no hint of an amorphous phase. Poor ionic conductivity is also observed for [Li⊂2.2.2][$CF_3SO_2NCH_2$-18-

(48) Doan, K. E.; Heyen, B. J.; Ratner, M. A.; Shriver, D. F. *Chem. Mater.* **1990**, *2*, 539.
(49) Vogel, H. *Phys. Z.* **1921**, *22*, 645.
(50) Tamman, G.; Heese, W. *Z. Anorg. Allg. Chem.* **1926**, *156*, 245.
(51) Fulcher, G. S. *J. Am. Ceram. Soc.* **1925**, *8*, 339.
(52) Dillon, R. E. A.; Shriver, D. F. submitted to *Solid State Ionics*.

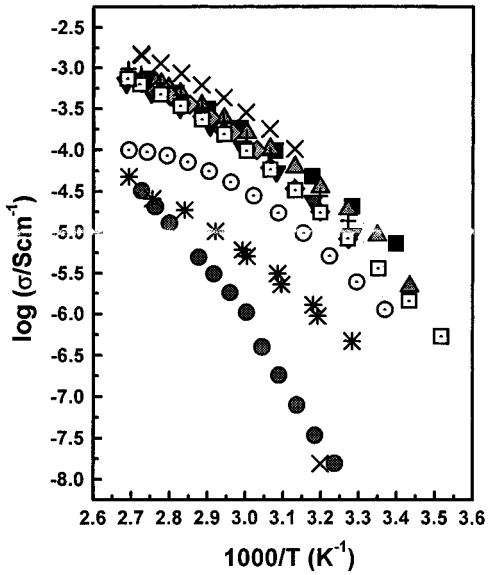

Figure 3. Temperature-dependent ionic conductivities (σ) of 1:1 ratios of Li[R−NSO_2CF_3] complexes with 2.2.2-cryptand: [LiMPSA⊂2.2.2] (■), [LiTFSI⊂2.2.2] (●), [LiMESA⊂2.2.2] (▲), LiDMESA⊂2.2.2] (▼), [LiIPSA⊂2.2.2] (◆), [LiESA⊂2.2.2] (+), [LiTFESA⊂2.2.2] (×), [Li18−C-6MSA⊂2.2.2] (*), [LiAMPSA⊂2.2.2] (□), and [LiTHFSA⊂2.2.2] (⊙).

C-6] which is analogous to the [Li⊂18-C-6][CF_3SO_2-NCH_2-18-C-6] complex.

Crystal Structure of Li[$CF_3SO_2N(CH_2)_2OCH_3$]. A single-crystal X-ray structure determination reveals that Li[$CF_3SO_2N(CH_2)_2OCH_3$] consists of one-dimensional arrays of interconnected eight-membered rings similar to the arrays observed in the Li[$CF_3SO_2N(CH_2)_3$-OCH_3] structure.[26] Figure 4 illustrates the coordination of the lithium cation by nitrogen and ether oxygen from one anion plus two sulfonyl oxygen atoms from each of two different anions. This lithium coordination environment is the same as that seen in the Li[$CF_3SO_2N(CH_2)_3$-OCH_3] structure. The similarity in structure between these salts coupled with the differences in thermal and spectroscopic data beg the question of why does Li[CF_3-$SO_2N(CH_2)_2OCH_3$] not form a complex with 18-C-6 comparable to the amorphous complex [Li⊂18-C-6][CF_3-$SO_2N(CH_2)_3OCH_3$]?

The smaller bond angles around the lithium cation for the Li[$CF_3SO_2N(CH_2)_2OCH_3$] structure (Table 5) reflect a more compact structure with the shorter alkyl chain. For example, the Li(0)−O(3)-C(3) bond angle, 108.3°, for Li[$CF_3SO_2N(CH_2)_2OCH_3$] is significantly smaller than the analogous Li−O−C angle, 123.6°, in Li[$CF_3SO_2N(CH_2)_3OCH_3$]. Similarly, the C(2)−N(1)−Li-(0) bond angle, 108.5°, for Li[$CF_3SO_2N(CH_2)_2OCH_3$] is less than the analogous bond angle, 119.4°, for Li[CF_3-$SO_2N(CH_2)_3OCH_3$]. The smaller bond angles are reflected in longer lithium−oxygen and nitrogen bond lengths (Table 6). For example, Li[$CF_3SO_2N(CH_2)_2$-OCH_3]−Li(0)−N(1), 2.013 Å, has a longer bond in comparison to Li[$CF_3SO_2N(CH_2)_3OCH_3$]−Li−N, 1.990 Å. Similar results are observed for the Li−O (sulfonyl oxygen) bond in Li[$CF_3SO_2N(CH_2)_2OCH_3$]−Li(0)−O(1), 1.928−1.943 Å compared to Li[$CF_3SO_2N(CH_2)_3OCH_3$]−Li−O, 1.915−1.919 Å. The shortening of the alkyl chain is best reflected in the Li−O (ether oxygen) bond. This is confirmed by comparing the Li(0)−O(3), 1.978 Å (Li[$CF_3SO_2N(CH_2)_2OCH_3$]), bond lengths to the Li−O, 1.943 Å (Li[$CF_3SO_2N(CH_2)_3OCH_3$]), values.

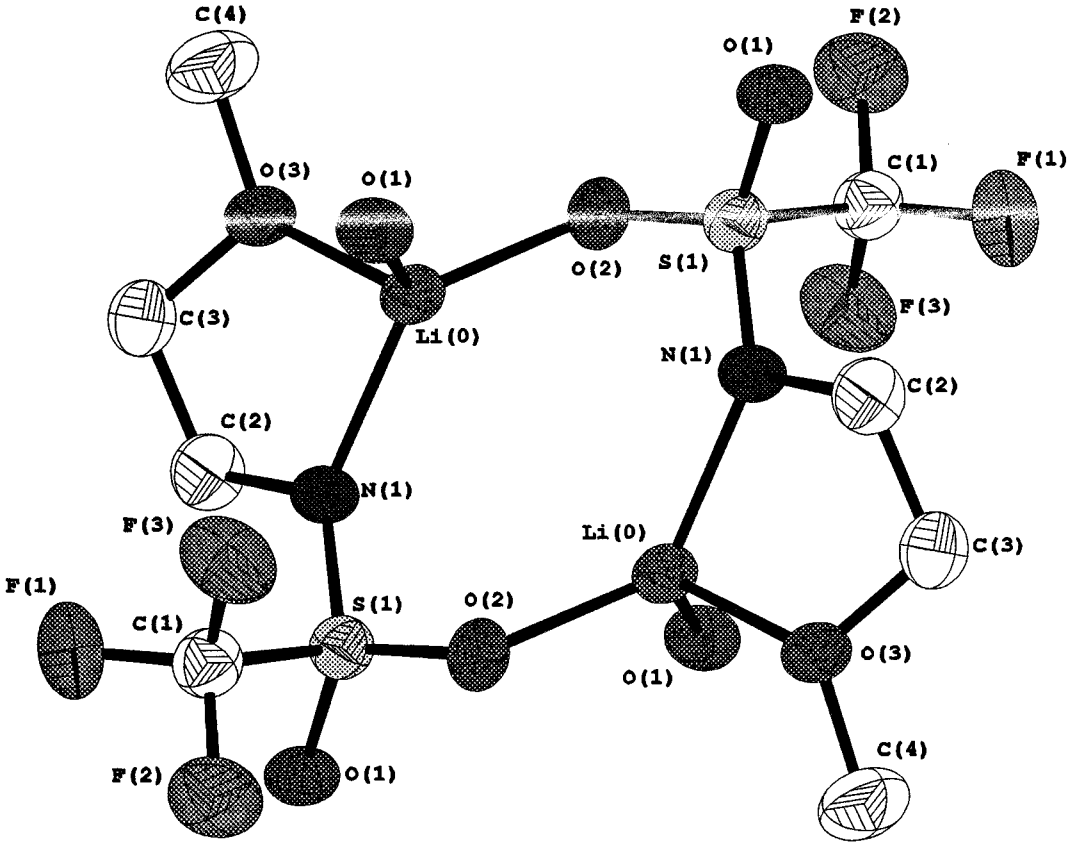

Figure 4. Coordination environment of the lithium cation in Li[$CF_3SO_2N(CH_2)_2OCH_3$].

Table 5. Bond Angles (deg) for $Li[CF_3SO_2N(CH_2)_2OCH_3]$

atom	atom	atom	angle	atom	atom	atom	angle
O1	S1	O2	116.9(2)	O1	S1	N1	117.0(2)
O1	S1	C1	100.7(2)	O2	S1	N1	110.2(2)
O2	S1	C1	101.3(2)	N1	S1	C1	108.6(2)
S1	O1	LI	142.3(3)	S1	O2	LI	126.2(3)
C3	O3	C4	112.9(4)	**C3**	**O3**	**LI**	108.3(3)
C4	O3	LI	118.6(3)	S1	N1	C2	119.3(3)
S1	**N1**	**LI**	131.3(3)	**C2**	**N1**	**LI**	108.5(3)
S1	C1	F1	110.4(4)	S1	C1	F2	111.7(4)
S1	C1	F3	112.1(4)	F1	C1	F2	106.4(4)
F1	C1	F3	108.4(4)	F2	C1	F3	107.7(4)
N1	C2	C3	107.7(4)	N1	C2	H1	109.6
N1	C2	H2	109.8	C3	C2	H1	110.0
C3	C2	H2	110.2	H1	C2	H2	109.4
O3	C3	C2	107.3(4)	O3	C3	H3	109.9
O3	C3	H4	110.0	C2	C3	H3	109.9
C2	C3	H4	110.1	H3	C3	H4	109.6
O3	C4	H5	109.2	O3	C4	H6	109.5
O3	C4	H7	109.3	H5	C4	H6	109.7
H5	C4	H7	109.4	H6	C4	H7	109.9
O1	LI	O2	109.0(4)	O1	LI	O3	110.1(4)
O1	LI	N1	114.1(4)	O2	LI	O3	107.3(4)
O2	**LI**	**N1**	127.9(5)	**O3**	**LI**	**N1**	84.2(3)

The crystal structure data indicate the subtle bond angle and bond length differences between $Li[CF_3SO_2N(CH_2)_2OCH_3]$ and $Li[CF_3SO_2N(CH_2)_3OCH_3]$. One striking feature of the $Li[CF_3SO_2N(CH_2)_2OCH_3]$ structure is its similarity to the lithium environment within a macrocycle (see Figure 4). This comparison is supported by the Raman band at 868 cm^{-1} in the spectra of $Li[CF_3SO_2N(CH_2)_2OCH_3]$ which occurs in a region typically assigned to the ring breathing mode of crown ethers around a cation. The interaction of the lithium cation with the CH_2CH_2-O constituent of the $[CF_3SO_2N(CH_2)_2OCH_3]^-$ anion may be responsible for the differences observed between the $Li[CF_3SO_2N(CH_2)_2OCH_3]$ and $Li[CF_3SO_2N(CH_2)_3OCH_3]$ salts.

Table 6. Bond Lengths (Å) for $Li[CF_3SO_2N(CH_2)_2OCH_3]$

atom	atom	distance	atom	atom	distance
S1	**O1**	**1.441(3)**	**S1**	**O2**	**1.445(3)**
S1	**N1**	**1.523(4)**	S1	C1	1.834(5)
F1	C1	1.334(5)	F2	C1	1.341(5)
F3	C1	1.318(5)	**O1**	**LI**	**1.928(8)**
O2	**LI**	**1.943(9)**	O3	C3	1.408(5)
O3	C4	1.429(5)	**O3**	**LI**	**1.978(7)**
N1	C2	1.485(5)	**N1**	**LI**	**2.013(8)**
C2	C3	1.516(6)	C2	H1	0.95
C2	H2	0.95	C3	H3	0.95
C3	H4	0.95	C4	H5	0.95
C4	H6	0.95	C4	H7	0.95

Summary

Thermal analysis of lithium salt complexes with 18-C-6 and 2.2.2-cryptand macrocycles clearly indicate that ionic glass formation is promoted by unsymmetrical anions having the general formula $[R-NSO_2CF_3]^-$ (where R contains an ether oxygen). Subtle variations in the structure of the anion significantly affect the properties of the salt complexes. In general, glass formation is favored by a mismatch between the cation size and that of the macrocyclic cavity. Asymmetry of the anion and the presence of ether oxygens in the anion also promote glass formation.

Acknowledgment. This research was supported by the MRSEC program of the National Science Foundation (DMR-9632472) at the Materials Research Center of Northwestern University.

Supporting Information Available: Text describing the syntheses and characterization of the compounds studied, tables of crystallgraphic data and bond lengths and angles for $Li[CF_3SO_2NCH_2CH_3]\cdot 1/2THF$, and figures showing parts of the structure of $Li[CF_3SO_2NCH_2CH_3]\cdot 1/2THF$ (PDF). This material is available free of charge via the Internet at http://pubs.acs.org.

CM000824F